Calibration Report of the EFW Measurements in the Cluster Active Archive (CAA)

prepared by

Yuri Khotyaintsev

1 Introduction

This document describes calibration results and procedures of the CSA products from the EFW instrument.

2 Instrument Description

A detailed description of the EFW instrument can be found in *Gustafsson et al*. (1997). We first briefly describe the raw quantities measured by the instrument, which correspond to Level 1 products in the CSA. The detector of the instrument consists of four spherical sensors numbered 1 to 4 deployed orthogonally on 44-meter-long wire booms in the spin plane of the spacecraft, as illustrated in Figure 1. The potential drop between two sensors, separated by

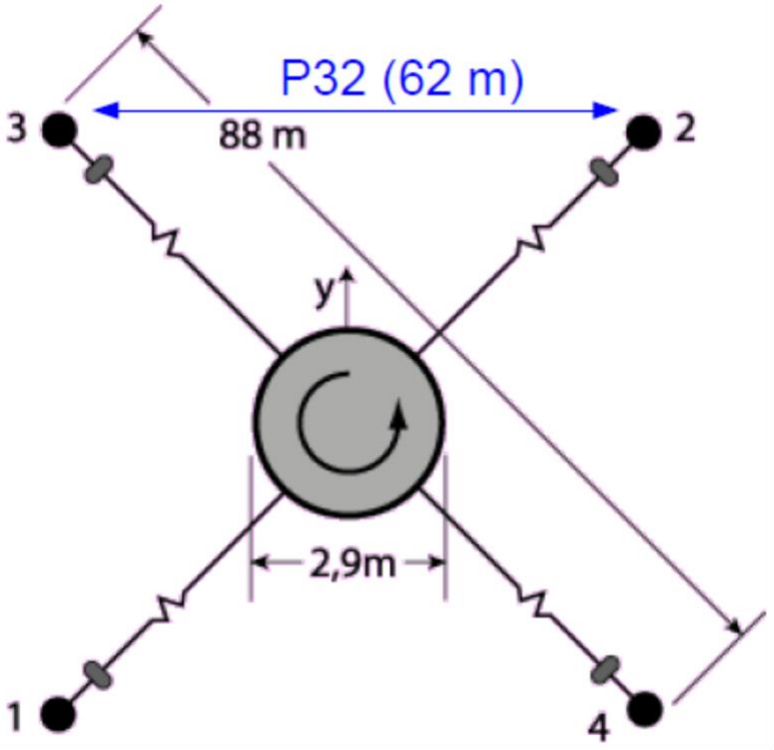

Figure 1: The EFW experiment

88 m tip-tip (62 m in case of P32), is measured to provide an electric field measurement (CSA dataset L1_E). The probe difference signals are normally routed through 10 Hz low-pass filters if sampled at 25 s^{-1}, and through 180 Hz low-pass filters when sampled at 450 s^{-1} (see "EFW non-standard operations dataset" in Section 10 for the exceptions). The potential

difference between each sensor and the spacecraft (CSA dataset L1_P1) is measured separately with a sampling frequency of 5 s^{-1} after routing through low-pass filters with a cut-off frequency of 10 Hz.

The EFW instrument measures the electric field only in the spacecraft spin plane; therefore, a spin-plane-oriented coordinate system is best suited for scientific studies involving the electric field. The **ISR2** (Inverted Spin Reference) system, also known as **DSI** (Despun System Inverted), is such a system. The X and Y axes are in the spin plane, with X pointing as near sunward as possible and Y perpendicular to the sunward direction, positive towards dusk. The Z-axis is along the (negative) spacecraft spin axis, pointing towards the north ecliptic pole. The coordinate system is called "Inverted" because the actual spin axis of Cluster is pointing towards the south ecliptic. The difference between ISR2 (DSI) and the GSE (Geocentric Solar Ecliptic) is a tilt of 2 to 7 degrees of the Z-axis performed in order to avoid shading of the EFW probes by the spacecraft. The exception is the May 2008 "tilt campaign", when the tilt angle on C3 can be up to 45 degrees.

3 Measurement Calibration Procedures

Spacecraft potential data (probe-to-spacecraft, not the plasma-to-spacecraft potential, see *Cully et al. 2007*) in the CSA do not require any special calibration. L2_P is usually computed as the average of all four probes; if one or two probes are missing, it is calculated as the average of two opposing probes, or only one if these probes are non-opposing. If only one probe is available, L2_P is given by the potential of that probe. In case of probe saturation due to high bias current (see "***Error! Reference source not found.***" in Section 4), we switch from averaging to using the maximum of all available probes, which gives the best estimate of the spacecraft potential.

Here, we describe the processing chain of the electric field data. At the initial stage of production we remove intervals with: bad data due to issues with electronics, probe saturations due to low plasma density, and non-optimal bias current settings. Usually, only a few minutes of data are removed from each orbit for these reasons. However, large data gaps may occasionally occur. If the spacecraft is in the solar wind we attempt to correct for the wakes usually present in the raw data (see "***Error! Reference source not found.***").

3.1 Spin fitting

In the presence of a constant ambient electric field, the raw data signal (probe potential difference) is a sine wave, with its amplitude and phase determining the electric field magnitude and direction. A *least-squares fit* to the raw data of the form

$$y = \boldsymbol{A} + \boldsymbol{B} \sin(\omega t) + \boldsymbol{C} \cos(\omega t) + \boldsymbol{D} \sin(2\omega t) + \boldsymbol{E} \cos(2\omega t) + \ldots \quad (1)$$

is done once every 4 seconds ($2\pi/\omega \approx 4$ sec is the spacecraft spin period), and gives the following output:

- The sine and cosine terms, ***B*** and ***C*** (L3_SFIT dataset), are used to compute the 4-sec-resolution electric field in ISR2.
- The *raw data DC offset*, ***A***. Ideally, the raw data DC level should be zero, but small differences between the probe surfaces and the electronics create a DC offset. If not corrected, it shows up as a signal at the spin frequency in the despun electric field. The DER dataset is based on ***A*** (see section 3.2).
- The standard deviation of the raw data from the fitted sine wave (L3_E dataset).
- Higher order terms, ***D***, ***E***, ..., may be used for diagnostics of data quality (not delivered to the CSA).

The electric field (computed from ***B*** and ***C*** for one of the probe pairs) and the standard deviation are available in the CSA as Level 3 E.

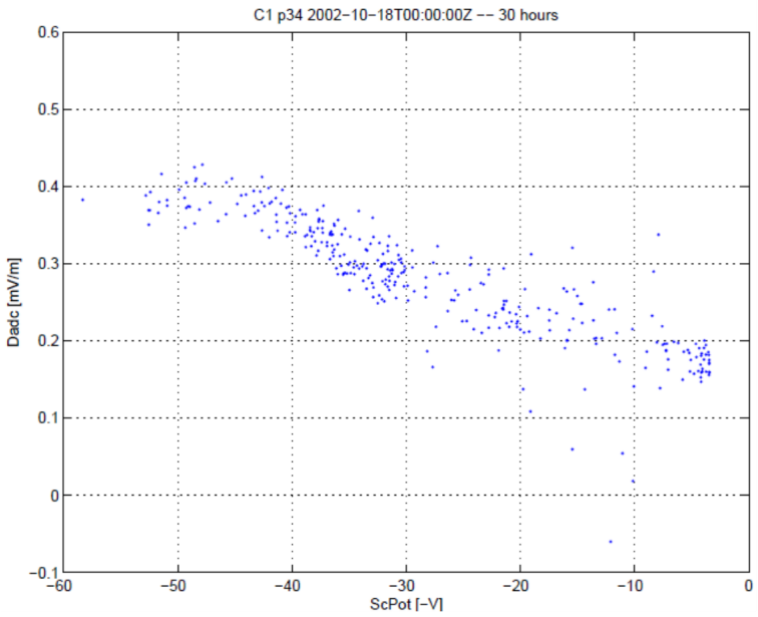

Figure 2: Raw data DC offset vs spacecraft potential

3.2 Raw data DC offset

The raw data DC offset (***A***) from both probe pairs is used for processing the full-resolution (L2) data. It is applied to P12/P32 and P34 prior to despinning and available in the CSA as the L3_DER product. Variations in the electric field cause small changes in the DC offset. DC offset also depends on the surrounding plasma environment, as illustrated in Figure 2. Therefore, we want a smoothed value and at the same time to track changes in the plasma environment, that is why the DC offset is smoothed using a weighted average over 7 spins using weights [.07 .15 .18 .2 .18 .15 .07] (see the EFW ICD). The smoothed offset is delivered to the CSA as the DER dataset. Intervals containing WHISPER pulses are blanked prior to despinning.

3.3 Delta offset

Another offset applied during despinning is the so-called Delta offset, which is based on the difference between the electric fields in ISR2 obtained from the least-squares fit procedure for the individual probe pairs P12/P32 and P34. This offset arises from differences in probe characteristics that evolve over time. Evolution of delta offsets for Cluster 2 for 2001-2005 is shown in Figure 3. The spikes in the plot are usually due to one of the probe pairs being partially saturated (removed during the offset computation). To get rid of these spikes and to account for the very slow evolution of the offset, we use a median over a 6-day period, corresponding to approximately 3 orbits (shown in green). The blue curve shows the offset values computed over 90-min (NM) or 30-min (BM1) intervals. On rare occasions when the delta offset changes rapidly, as for example after some of the maneouvres, we use manually

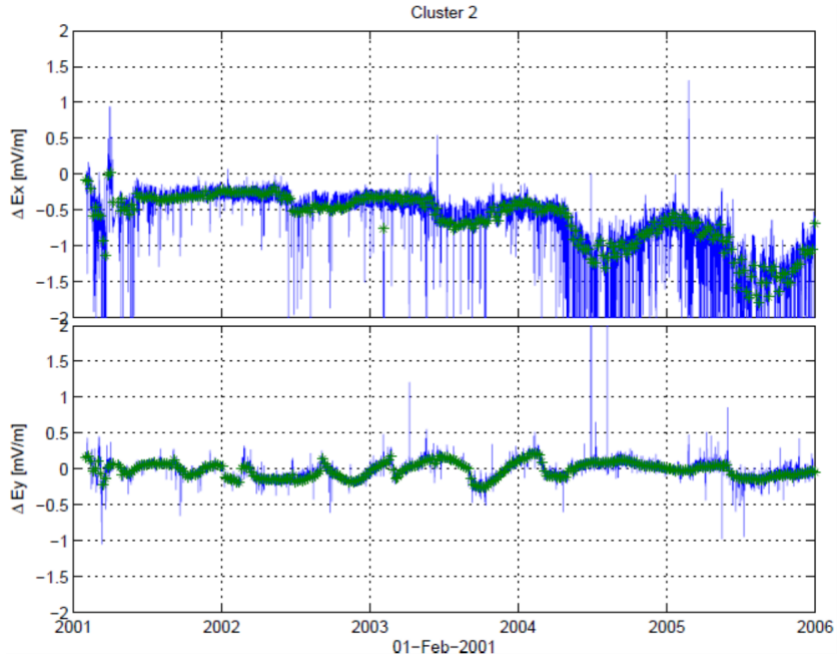

Figure 3: Delta offsets for Cluster 2

verified tabulated values. The delta offset is applied during the despin when L2_E is produced. The delta offset is always corrected on P12/32. The value applied is given in FILE_CAVEATS section of the CEF file:

```
ENTRY       =   "2007-12-02T00:00:00.000Z/2007-12-02T01:09:00.000Z
p12 offset (ISR2): dEx=0.21 dEy=-0.05"
```

3.4 Amplitude correction

At this stage, both the full-resolution (L2, from despinning) and 4-sec (L3, from least-squares fit) electric fields contain systematic errors, namely an amplitude factor and a DC offset, which need to be corrected for.

The ambient electric field is "short-circuited" by the presence of the spacecraft and wire booms. This is caused by the spacecraft potential, which is also the potential of the wire booms extending out to a large distance from the spacecraft. On the basis of simulations and comparisons with other Cluster instruments, it has been determined that the measured electric field magnitude needs to be multiplied by a factor of 1.1 (see "**Error! Reference source not found.**" in Section **Error! Reference source not found.** for more detail) to get the real electric field (see also *Cully et al. 2007*). However, this factor depends on the plasma environment and, in some cases, may deviate from the value used. In the case of Cluster, it can range from 1.0 to ~1.2, but is usually 1.1.

3.5 ISR2 DC offset

The spacecraft, wire booms, and probes emit photoelectrons, which create an excess of negative charge on the sunward side. This will be measured by the EFW instrument as a spurious sunward electric field, generally referred to as the sunward DC offset. Most of the time, the offset varies slowly with time and plasma conditions around the spacecraft, and is slightly different for the different spacecraft. However, rapid changes can also occur, for example, due to fast crossings of plasma boundaries or rapidly varying solar UV flux, which can both alter the satellite photoelectron cloud.

The magnitude of the offset is determined by comparisons with other measurements from the Electron Drift Instrument (EDI) and the Cluster Ion Spectrometry experiment (CIS). The values of the offsets that have been subtracted from the data in the CSA are given in the FILE_CAVEATS section of the CEF files. The photoelectron asymmetry responsible for the sunward DC offset, by definition, gives an offset in the sunward direction only. However, results of comparisons with other instruments have at times shown an offset of a fraction of mV/m also in the duskward direction, which is not yet well understood. In most cases, the duskward offset is negligible.

Prior to delivery to the CSA, we attempt to identify and mark intervals with suspected spurious fields in various magnetospheric regions (see "***Error! Reference source not found.***"

and "***Error! Reference source not found.***" in Section 10).

4 Measurement Processing Procedures

4.1 Issues due to electronics & instrument saturations

In this chapter, we describe the procedure we use to identify bad data caused by electronic issues. These include instrument misconfiguration, malfunction, digital saturation, etc. Data during such intervals cannot be recovered.

First, we remove all data within the 1-minute interval prior to (the timing of which is unknown) and the 3-minute interval after the EFW reset. Following the reset, EFW boots into default mode, which has non-optimal bias current settings. These settings are usually reprogrammed to nominal 2-3 minutes after a reset.

After this, we check the actual bias current measurements and disregard all data that have non-nominal settings. Nominal bias current setting for all years of operation can be found in "EFW User Guide", and actual bias current settings are included in the HK dataset.

Then we check for probe saturations. First, we look for probes and probe pairs "getting stuck," which is identified by a non-changing measurement for four consecutive points. Then we check for measurements being saturated due to low density when the probes reach the maximum digital value of 68 V.

Some additional intervals may be manually disregarded based on the "EFW non-standard operations database" (see caveats dataset C[1-4]_CQ_EFW_INST). These usually include maneuvres, bad telemetry packets, unusual sampling modes, and instrument settings. These intervals are marked in the quality information supplied with the electric field data: bits 0-6 set in the E_bitmask (see EFW User Guide). For such intervals, the data will typically contain the fill value, or there will be a data gap.

4.2 Detection of saturation due to high bias current in dense plasmas

Due to long-term evolution in probe characteristics, the nominal bias current setting of 140 nA began to cause saturation in the dense magnetosheath plasmas in spring 2004. The problem became more prominent in 2005, and the nominal setting was lowered to 100 nA. See EFW User Guide for more details. The saturated time intervals usually contain very large electric field spikes in every spin with amplitudes sometimes reaching the digital saturation level. We have developed an algorithm that detects such saturations based on spike amplitude, shape, etc. The algorithm is, in many ways, similar to the one used for detecting solar wind wakes. The algorithm in action is illustrated in Figure 4. The time intervals during which saturation was observed are marked by a red/green envelope. The saturated time intervals are blanked in the CSA because they typically contain useless measurements. These intervals are marked in the quality information supplied with the electric field data: bit 14 set in the E_bitmask (see the EFW User Guide).

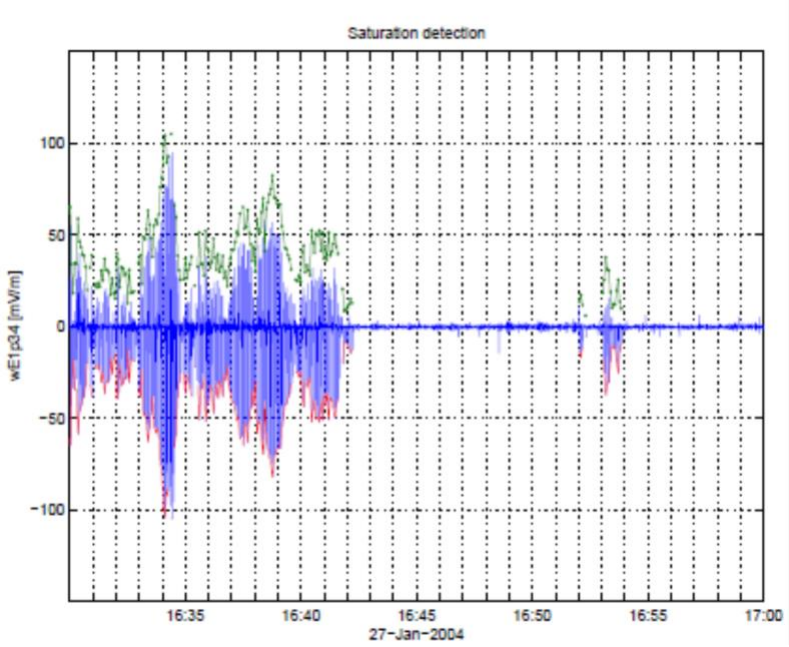

Figure 4: Detection of saturated intervals due to high bias current.

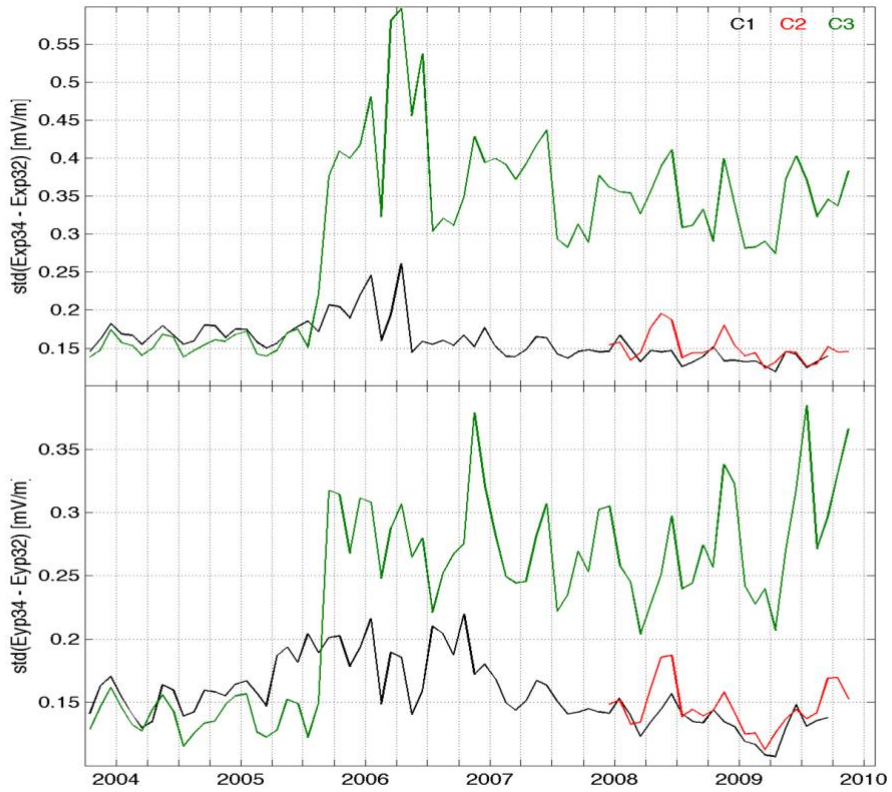

Figure 5: Difference between the spin fits from the long (p34 – 88m) and short asymmetric (p32 – 62m) probe pairs.

4.3 Measurements with an asymmetric probe configuration

To measure full-resolution electric fields with EFW, two probe pairs are required. The optimal situation is when the probe pairs are equally long, orthogonal, and symmetric with respect to the spacecraft. The spacecraft on which probe 1 failed after some period of operations (for exact times see) caveats dataset C[1-4]_CQ_EFW_INST are normally run in so-called “asymmetric mode”, e.g., the difference between probe pairs 2 and 3 is measured in addition to p34. Then p12 can be computed (on ground) from a combination of p32 and p34, and the normal processing procedure can be used.

However, this measurement has lower quality than “normal” p12 because p32 is shorter (62 m instead of 88 m) and is not symmetric with respect to the spacecraft. The spin fit data is practically not affected by this problem. Figure 5 shows the standard deviation of the

difference between the spin resolution electric fields obtained from the long p34 and the short p32 probe pairs. Here we have included data only from spacecraft spins with relatively quiet electric activity, i.e., when the standard deviation of the spin fit is below 0.3. One can see that the statistical difference between the spin fits for the long and short probe pairs is small, typically about 0.15 mV/m for C1 and C2, and for C3 before September 2005. Since September 2005, something has happened to C3, and it shows reduced data quality.

For the full-resolution electric field, using the short probe pair results in modulation at 2 times the spin frequency in the raw data, yielding signals at 1 and 3 times the spin frequency (about 0.25 and 0.75 Hz) in the despun data (see the upper panel in Figure 6). This

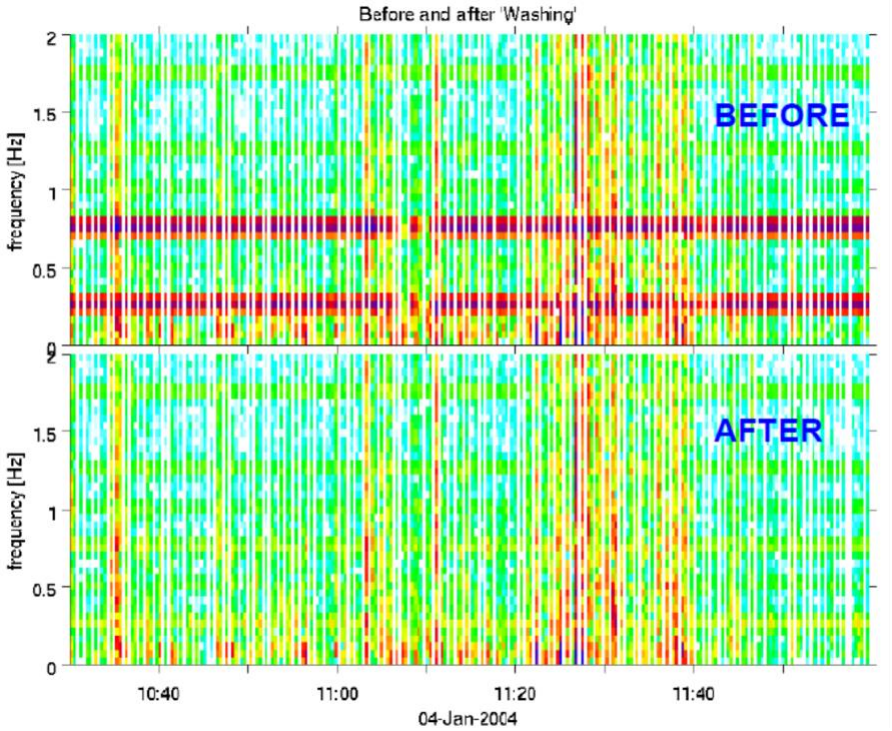

Figure 6: Original and "washed" data in the asymmetric configuration

modulation becomes apparently prominent when electric fields become small.

We have tried two algorithms for cleaning (we use the term “washing”) this modulation in the data. The first algorithm, referred to as “old”, computed the FFT of the p32 data, removed the peak at 2 times the spin frequency by interpolating the spectrum, and then computed the inverse FFT. The results from this method were good but not satisfactory; they caused

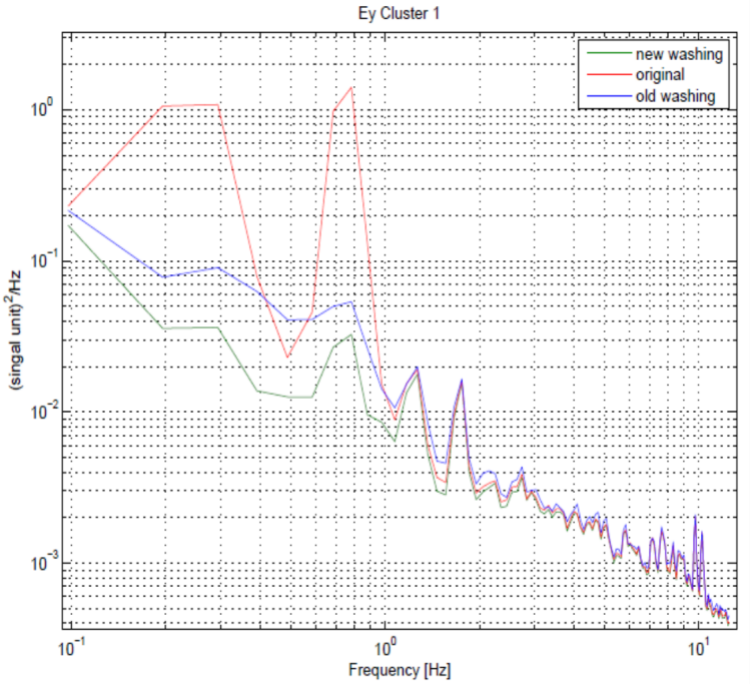

Figure 7: E spectrum before and after washing. The spacecraft spin frequency is ~0.25 Hz.

problems at the edges of the FFT window. That is why we developed a new algorithm, referred to as “new”, which is simply removing the signal at 2 times the spin frequency obtained from spin fitting (terms ***D*** and ***E*** in Equation 1). The spectra and time series produced by these two algorithms are shown in Figures 7 and 8.

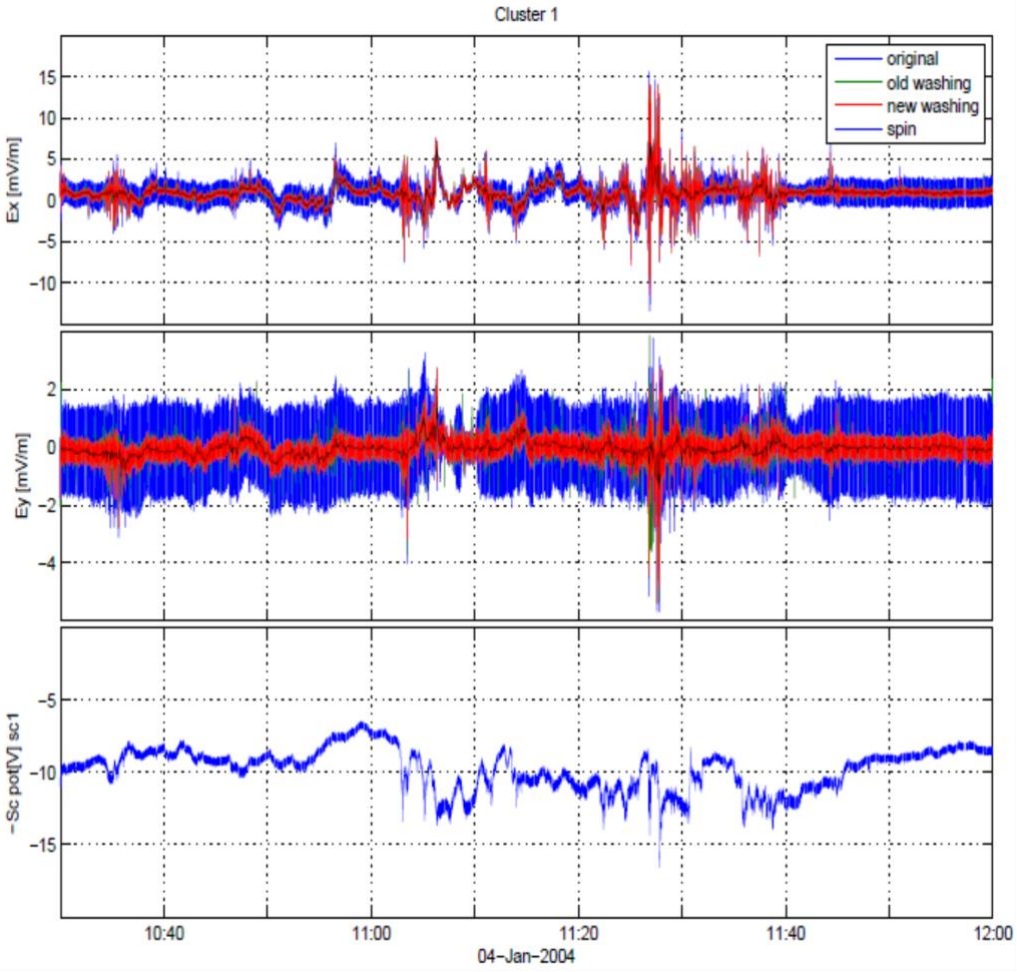

Figure 8: Timeseries of the despun electric field resulting from raw and washed data.

4.4 Cleaning wakes in the solar wind

In the solar wind, we remove wakes. A detailed description of the procedure can be found in *Eriksson et al. (2007)*. Wakes are routinely removed in the solar wind and the affected spins have bit 10 set in the E_bitmask for the electric field datasets (see the EFW User Guide). This is done before the spin fitting procedure.

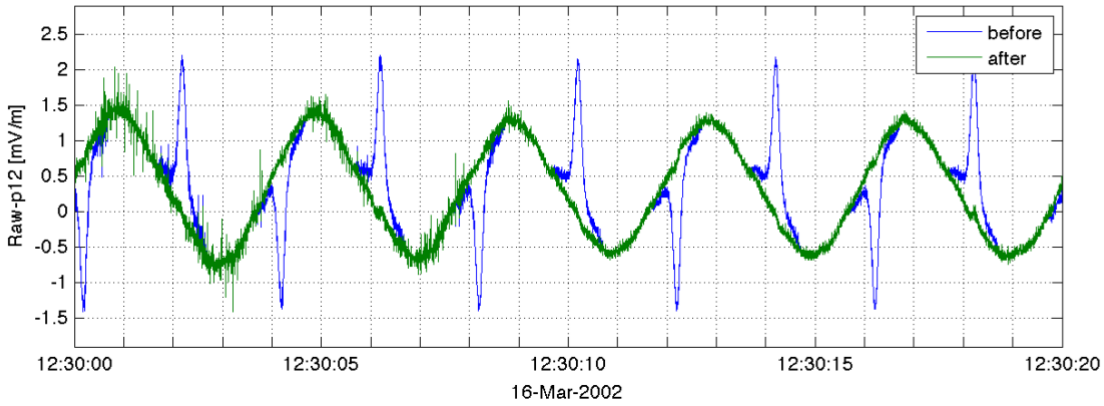

Figure 9: Solar wind wake removal.

4.5 Detection of spurious electric fields in the plasmasphere

During comparisons of electric field measurements made by EFW and EDI in the inner magnetosphere, it was found that EFW sometimes measures a spurious field of the order of 1-2 mV/m, mostly in the sunward direction (Figure 10, see also Figure 1c in *Puhl-Quinn et al. 2008*). The raw data signal is often non-sinusoidal (top panel). This problem is not quantitatively understood, but apparently depends on simultaneously acting phenomena:

(a) the dense plasmaspheric plasma can sometimes be so high as to give a random electron current to the probes almost as large as the applied bias current, driving the probe away from its vacuum potential with respect to the plasma;

(b) the wake created by the spacecraft makes the random current and the resulting error dependent on the spin phase and hence gives an apparent DC field in a non-spinning reference frame; and

(c) small differences in probe surfaces and bias circuitry will make this effect slightly different between the probes, further complicating the result.

A first principles error treatment is therefore complex. Nevertheless, an empirical algorithm has been developed to detect the bad data. We have developed an algorithm to detect such spurious fields by comparing the electric field measured by EFW to the corotation electric field. If the 1-minute averaged measured field deviates from corotation by more than 1 mV/m, such an interval will be marked as “plasmaspheric wake” in the quality information supplied with electric field data. This Algorithm is applied only for altitudes below 6 R_E and when the negative of the spacecraft potential exceeds -1.5 V, e.g., really only in very dense

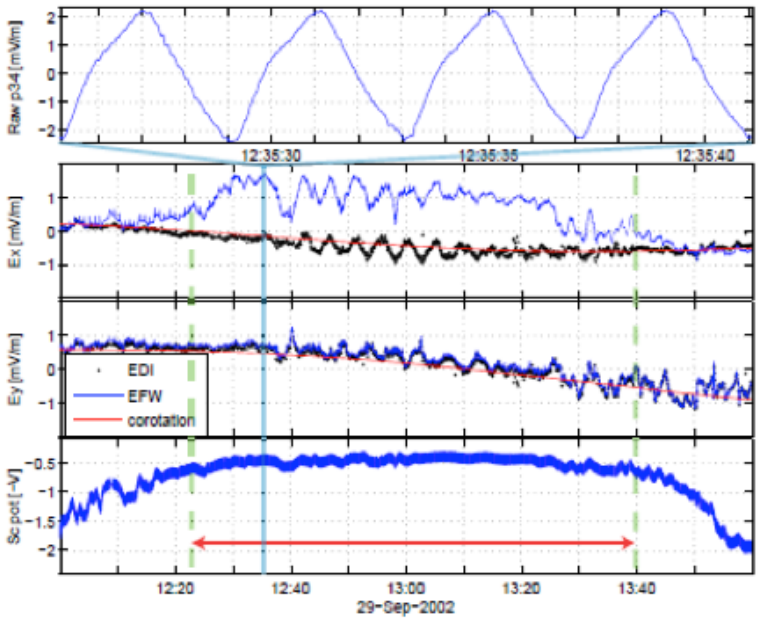

Figure 10: Spurious fields in the plasmasphere

corotating plasmasphere. We need to compare to corotation because the EDI measurements are not always available and never on C4. The algorithm in action is illustrated in Figure 10. The panes show the ISR2 components of electric fields measured by EFW and EDI, as well as the corotation fields. The upper panel shows a large deviation of EFW Ex from both the corotation and EDI measurements, and this data interval will be marked as "wake" in the quality data, with bit 12 set in the E_bitmask for the electric field datasets (see the EFW User Guide). One should note that the spurious field may also appear in the ISR2 Y direction.

4.6 Detection of cold ion flow wakes

One of the most problematic regions for measuring electric fields with double probe instruments (as EFW) are regions with low plasma density and flowing cold plasmas. In the low-density plasma encountered, for example, in the tail lobes, above the polar caps, and in

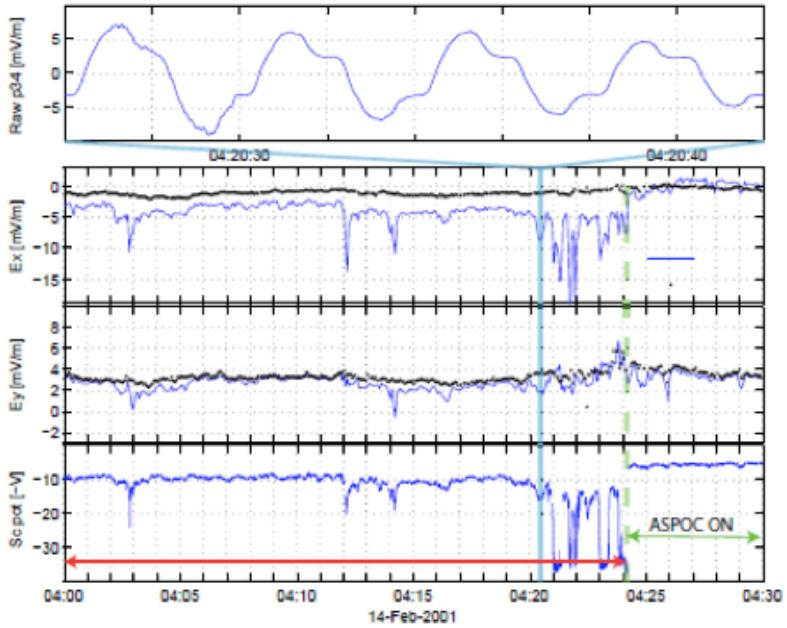

Figure 11: Wake detection in low density plasmas (EFW-blue, EDI-black).

the low latitude dayside magnetosphere, the spacecraft potential is usually of the order of several tens of volts. A cold ion population flowing in such plasma environments will see effectively much thicker booms (several meters instead of a few mm), creating a large negatively charged wake behind the booms in the direction of flow (*Eriksson et al. 2006, Engwall et al. 2006*).

Figure 11 shows an example of such a wake, defined by a large deviation of E_x measured by the EFW and EDI. When ASPOC is operating, the spacecraft potential is kept much lower, and the problem of wakes caused by cold ion drift is much less severe. In comparison to the solar wind wake, the ion drift wake is broader and more diffuse. For a relatively small wake, the raw data are non-sinusoidal (see top panel in Figure 11). For a large wake, they can become sinusoidal again and look very similar to those created by a real ambient electric field.

The CSA production software attempts to detect such ion wakes by analyzing a combination of parameters, such as spacecraft potential, magnetic field direction, and the relationships among different electric field components. For small magnetic field elevations (B direction within 15 degrees of the spin plane), we check the ratio of the components of E along the projection of B into the spin plane and perpendicular to it. For larger elevations, we look at the ratio between the measured (spin plane) and unmeasured (perpendicular to the spin plane) components of $E_\perp$, where $E_\perp$ is computed under the assumption of a zero parallel electric field, $\mathbf{E}\cdot\mathbf{B} = 0$. Higher ratios indicate a greater likelihood that the wake is present in the data. At present, there is no algorithm to correct the data, and the bad intervals are marked in the quality information supplied with Level 2 and Level 3 data: bit 11 is set in the E_bitmask (see the EFW User Guide). Since it can sometimes be difficult to distinguish these wakes from a real electric field, analysis of the electric field should be done with caution in regions with possible cold-ion drifts.

5 Results of Calibration Activities

Major calibration activities include determining the Raw Data Offset (L3_DER product) and Delta Offsets, as described in the previous section.

5.1 EFW noise and sensitivity

Here, we describe the expected sensitivity and noise characteristics of the EFW data. Figure 12 shows a typical spectrum of Ey ISR2 measured by EFW in the solar wind; in this example, the E-field is sampled at 450 Hz (BM1) and then low-pass filtered at 180 Hz. In the solar wind, the electric field has one of the lowest signal levels compared to all the regions encountered by Cluster, and the EFW sensitivity level is often reached at frequencies above several Hz. We choose to study the Ey ISR2 component on C4, which is one of the cleanest signals EFW available on Cluster. The expected spectrum has a power-law shape, corresponding to a straight line on a log-log plot. One can see that the measured spectrum is

approximately a power law at low frequencies and begins to flatten at several Hz, reaching the sensitivity floor of ~5×10^-6 $(mV/m)^2/Hz$ at frequencies above 20 Hz.

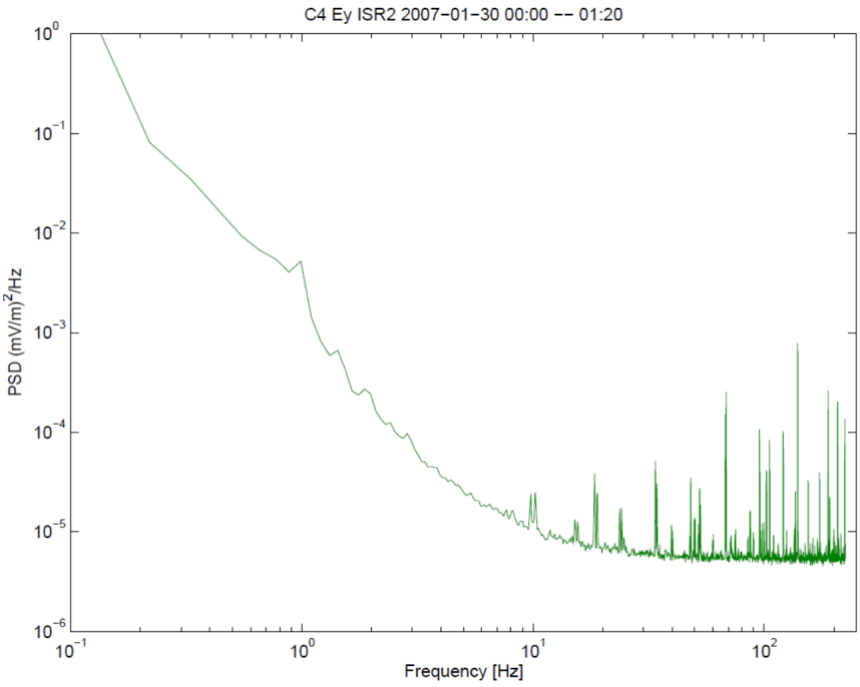

Figure 12: Ey spectrum in the solar wind.

Another striking feature in Figure 12 is the presence of sharp peaks at frequencies above 10 Hz. These peaks are due to a high-frequency signal within the EFW electronics, aliased down and unaffected by the 180 Hz low-pass filter.

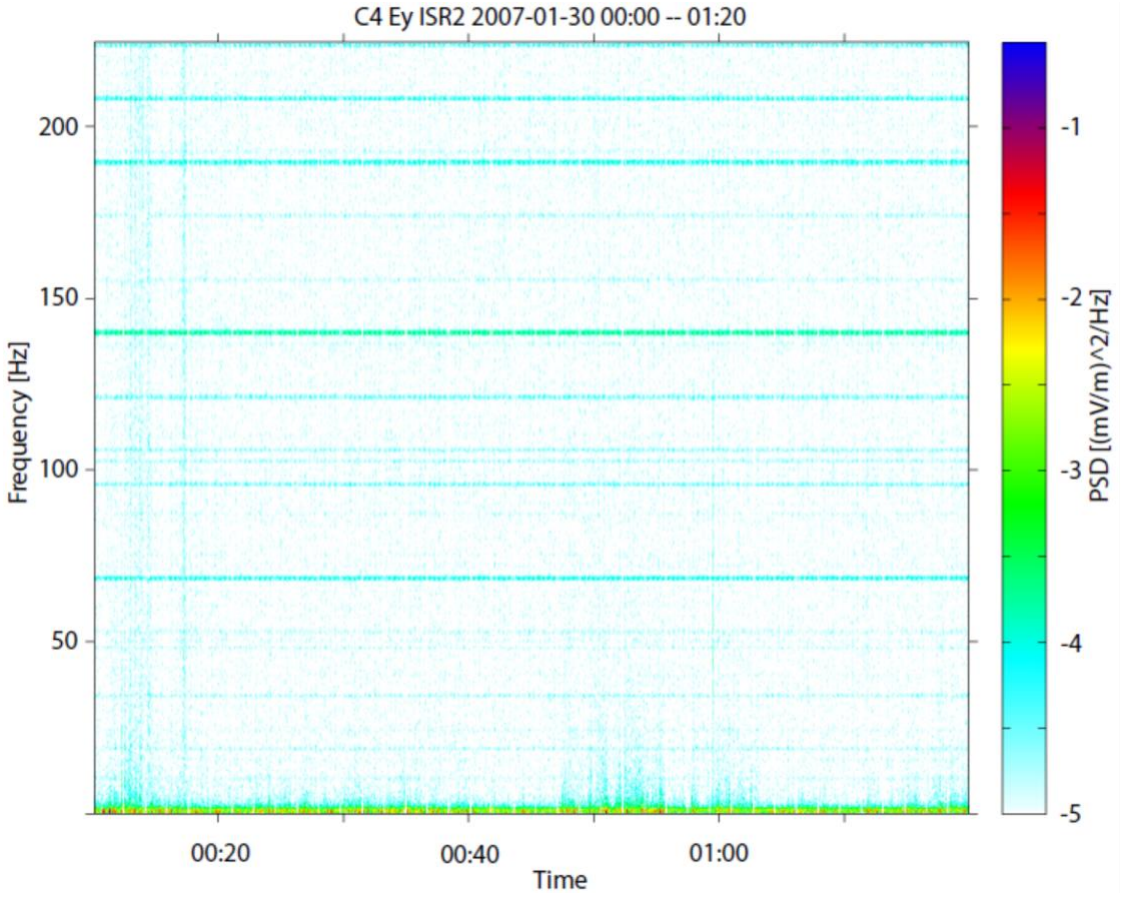

Figure 13: Time-frequency spectrogram of Ey in the SW

Figure 13 shows a time-frequency spectrogram of the same data, and one can clearly see that the peaks in the spectrum correspond to the narrow spectral lines. In some cases, a small frequency drift in these lines can be observed, possibly due to heating/cooling of the electronic components as the spacecraft enters a plasma region with different properties. These lines could, in principle, be removed from the data, but it does not make much sense, since the actual signal level is significantly below the sensitivity level in this case.

We have studied the sensitivity of EFW by examining the frequency range from 70 to 180 Hz. The BM1 EFW data for 2001-2008 were split into 30-minute intervals, then a spectrum was computed over every 4 seconds of data, the spikes were thrown away, and the mean value was computed in the 70-180 Hz range. Then we selected the lowest value in the 30-minute interval. The result for probe pair 12/32 for all spacecraft is plotted in Figure 14. One can see

that the sensitivity level is ~2×10^-6 $(mV/m)^2/Hz$ at the beginning of the mission. Then it increases by a factor of 10-20 after probe 1 gets broken on C1, C3, and C2.

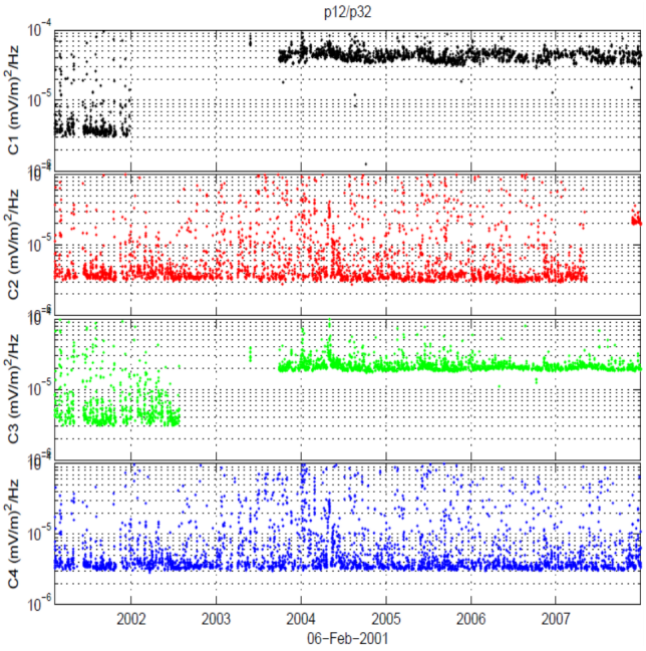

Figure 14: Evolution of sensitivity level on p12/p32

The results for probe pair 34 are shown in Figure 15. Here, the initial level is about 5 times higher than for p12. The level gets slightly higher with the introduction of the EFW flight software version 2.4 (FSW 2.4) at the end of 2003, where the analog difference is replaced by digital in order to compute p32.

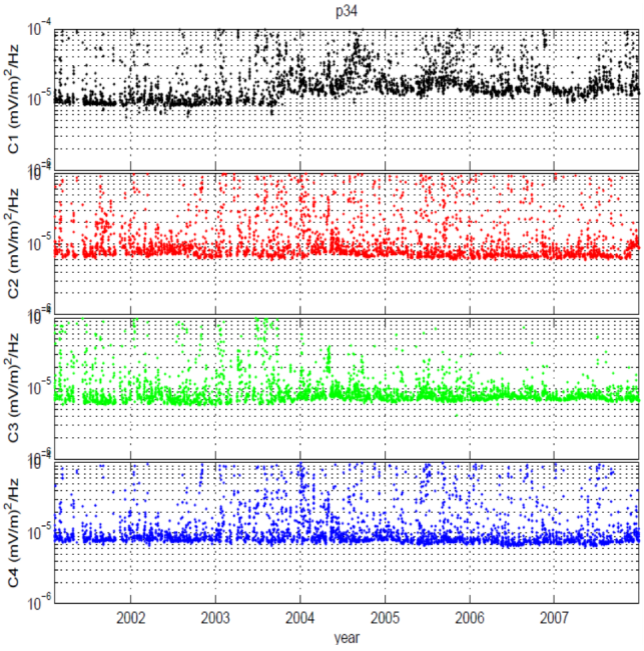

Figure 15: Evolution of sensitivity level on p34

6 Results of Cross-Calibration Activities

Cross calibration was mainly used to determine the amplitude correction factor for the electric field data and offsets in ISR2.

We have also performed a large "Cross-calibration study" in order to evaluate the quality of electric fields measured by different instruments.

6.1 ISR2 offsets and Amplitude correction factor

Our main assumption in the study of ISR2 offsets is that the offsets depend on the instrument configuration, spacecraft attitude and that the dependence on surrounding plasma parameters is weak, i.e. being in the same kind of plasma environment (for example plasmasheet) and having the same instrument settings and probe properties for two different time intervals, the difference for between ISR2 offsets for the two intervals must be within the uncertainty of the offset determination (several tenth of mV/m). As the offsets still depend on the plasma environment, we decided to split the dataset into two groups: "solar wind/magnetosheath" and "magnetosphere", corresponding to "cold and dense" and "hot and

rarefied" plasmas, respectively. To split every orbit into these two groups we have used the Shue magnetopause model (*Shue et al. 1997*) with realistic solar wind parameters measured by ACE.

6.1.1 Offsets in the solar wind and magnetosheath

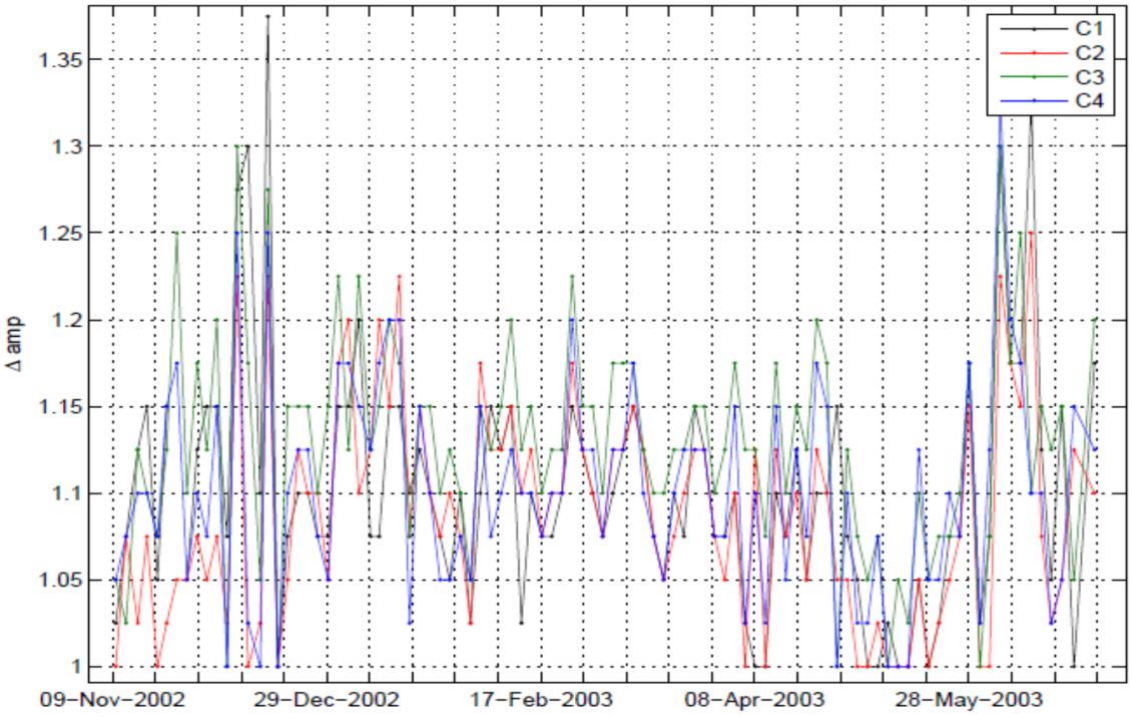

Figure 16: Amplitude correction factor in fall 2002 - spring 2003

6.1.1.1 Amplitude correction factor

First, we studied the amplitude correction factor (see Section **Error! Reference source not found.**, e.g., the factor by which the measured electric field amplitude needs to be increased in order to get the real electric field present in plasmas. The ambient electric field is "*short-circuited*" by the presence of the spacecraft and wire booms. This is caused by the spacecraft potential, which is also the potential of the wire booms extending out to a large distance from the spacecraft.

We have used the ISR2 Y components of the electric field to determine the amplitude correction factor. This component of E is generally free from offsets, and thus by comparing Ey from EFW and CIS-HIA, we are able to deduce the amplitude correction factor. Results of such computations for the spring season of 2002 are shown in Figure 16. Every point in the

plot corresponds to one orbit of data. One should note that the variations observed in the data are not due to changes in the factor, but rather to bad data and insufficient data coverage.

Based on simulations and comparisons with other Cluster instruments, it has been determined that the measured electric field magnitude must be multiplied by 1.1. We use this constant value throughout the entire mission. It is given as a dAmp parameter in the FILE_CAVEATS section in the CEF files for the electric field data.

6.1.1.2 ISR2 offsets

After we know the amplitude correction factor, we can determine the ISR2 offsets, which are simply the differences between the spin plane electric fields measured by EFW and CIS-HIA (VxB).

First, we perform the inter-spacecraft calibration under the assumption that all the spacecraft observe the same large-scale electric field, which is usually the case in the solar wind. Then, using CIS-HIA from C1 and/or C3 as reference data, we determine the ISR2 offsets for EFW for each spacecraft. We get one offset value per orbit.

The procedure can be controlled visually using the plot shown in Figure 17. The two upper panels show all the available EFW and CIS-HIA data (Ex and Ey in ISR2). Then we construct the *reference E-field* from the available CIS-HIA by averaging. This is possible because the difference between the spacecraft in the SW/MSH is small. Then we compute the difference between the EFW Ex on all spacecraft and the reference E-field, and plot it in the third panel. The average of the difference over the entire interval gives the local ISR2 offset. This offset is then applied to the EFW on different spacecraft. The resultant corrected and reference E-fields are plotted in the two bottom panels.

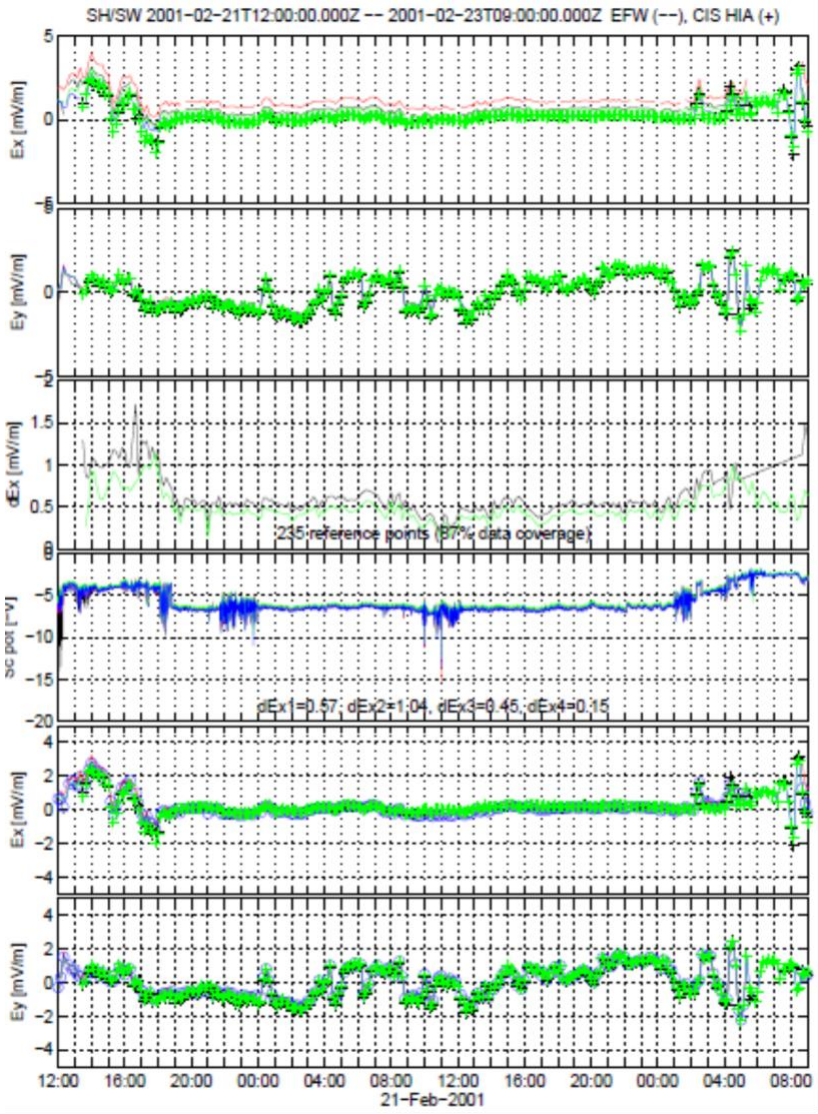

Figure 17: ISR2 offsets in the SW/MSH. The two lower panels show the electric field data to which the local offsets determined for this orbit have been applied.

We have conducted this analysis on all available solar wind and magnetosheath data, grouping the data into "solar wind periods" from November to June. The resulting ISR2 offsets for EFW on all Cluster spacecraft for 2003 are shown in Figure 18. It is evident that the distribution of offsets is quite centered around the mean. The scatter mainly results from poor data quality and limited data coverage.

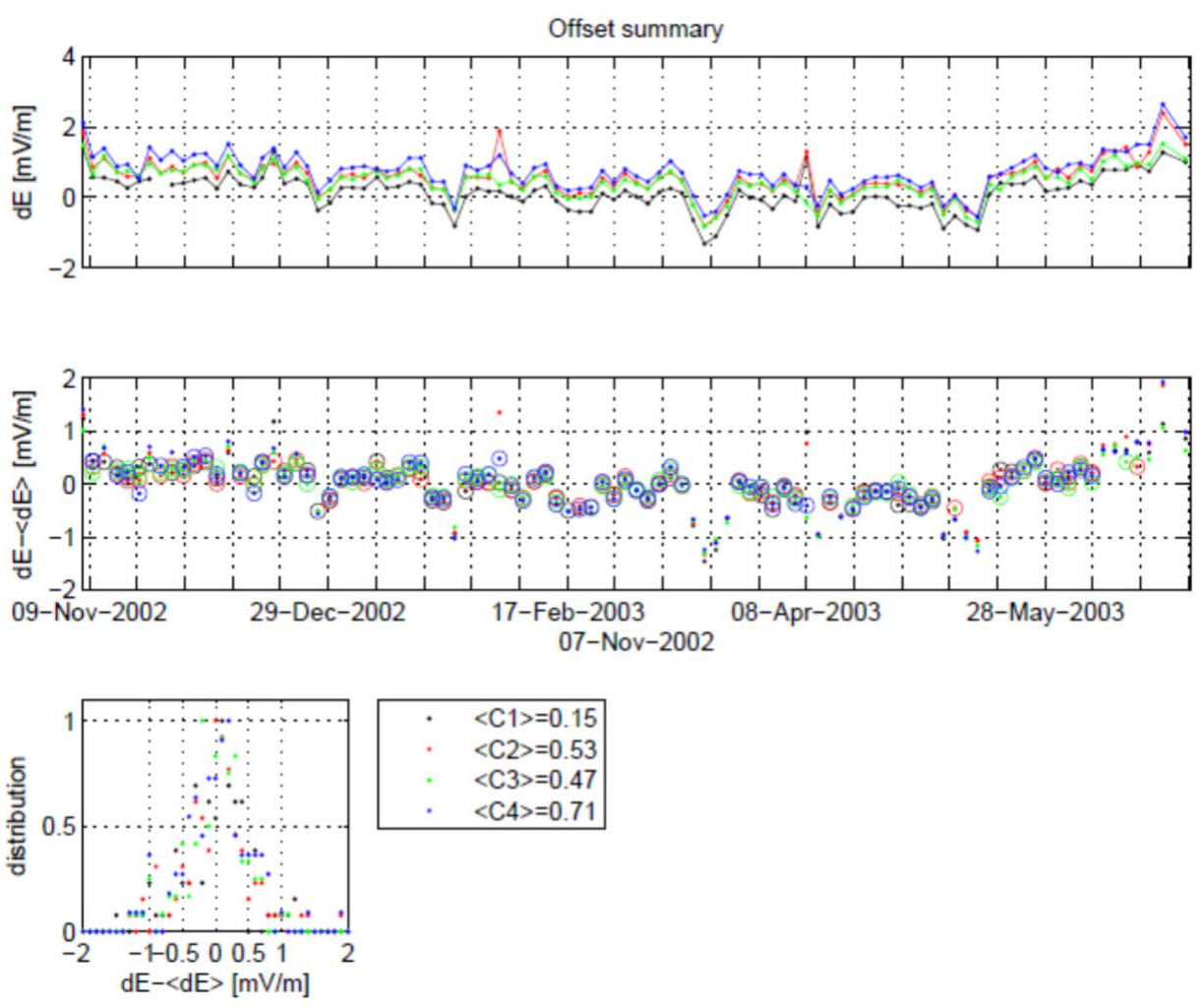

Figure 18: ISR2 offset summary (Ex) in the SW/MSH for spring 2003. The top panel shows the instantaneous offsets determined for each orbit. The middle panel shows the difference between the instantaneous offsets and the average "seasonal" offset, which is used in the CSA production (<C1>..<C4> in the panel below), and which is computed on the basis of the encircled points. The distribution of the difference is shown in the bottom-left panel.

Later, the offset values obtained by this automatic procedure are manually verified and, if necessary, corrected; the values applied are given in the FILE_CAVEATS section in the CEF files for the electric field data, for example:

```
ENTRY       =    "2007-12-02T00:00:00.000Z/2007-12-02T01:09:00.000Z
ISR2 offsets: dEx=0.85 dEy=0.00, dAmp=1.10"
```

gives the values of the ISR2 offsets and correction factor applied between 00:00 and 01:09.

6.1.2 Offsets in the magnetosphere

Determining offsets in the magnetosphere is significantly more complicated than in the solar wind/magnetosheath. Data from the other instruments, which could have been used as a reference, are of very low quality in large areas of the magnetosphere due to low counts or low magnetic fields (see "Cross-Calibration study"). Also, the EFW data are subject to frequent problems, such as electrostatic wakes.

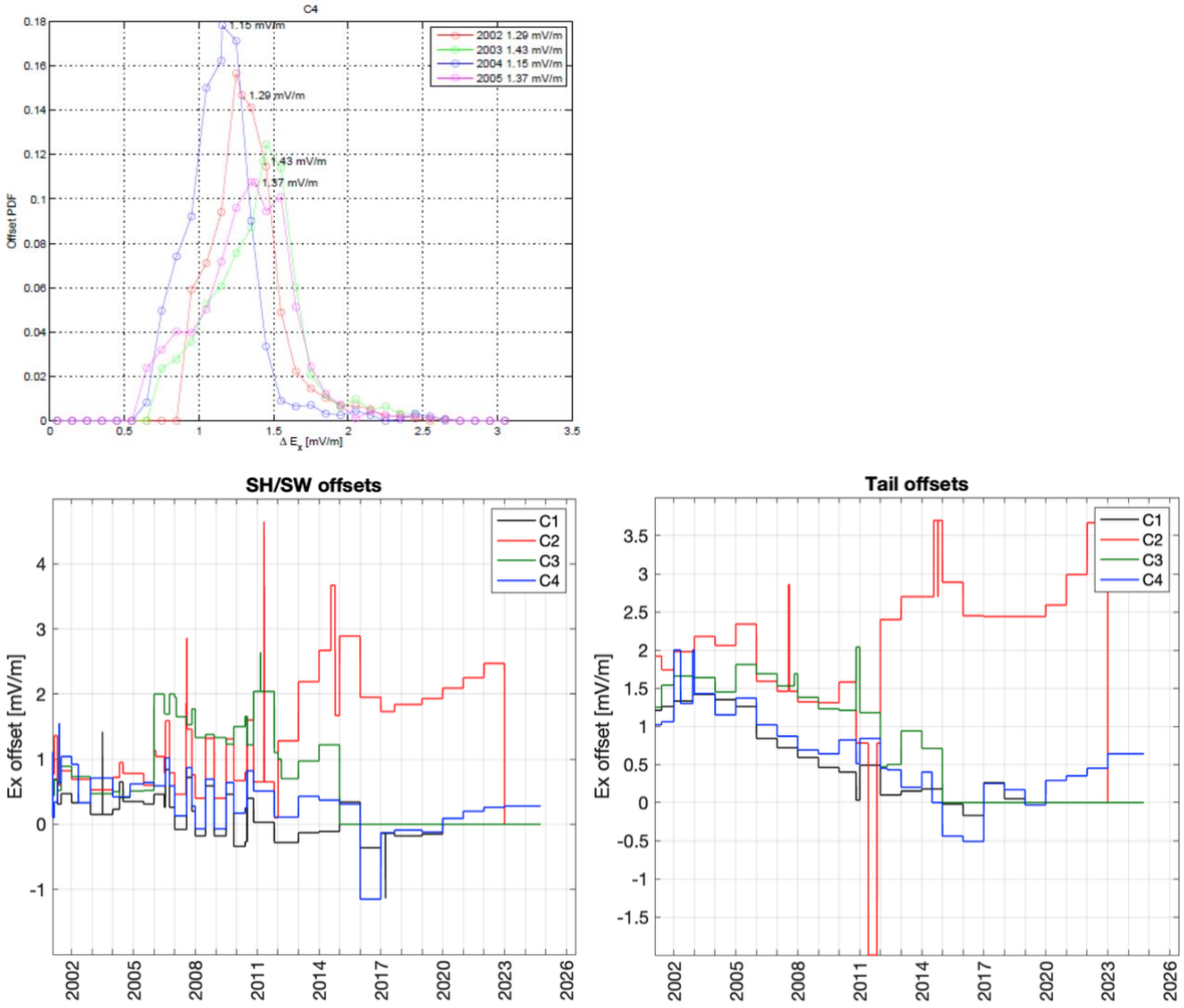

*Figure 19: **Above**: Example of statistical distributions of ISR2 X offsets for Cluster 4 in the magnetosphere. **Below:** Applied offsets on all s/c during the full mission, for solar wind/magnetosheath (left) and magnetosphere (right, denoted "tail").*

In the ISR2 offset determination procedure we decided not to use any reference data, but

rather use a condition of zero electric field <E_x>=0, as most of the times the electric fields are really very weak in the magnetotail (X_GSE < 0 and R > 5 R_E), and averaged over a tail season this should give a rather good estimate for the ISR2 X offset.

Results for Cluster 4 are summarized in Figure 19. One can see a prominent peak around 1.3 mV/m in all years; a group of points also shows broadening towards lower offset values. The nature of this broadening can be understood by plotting the ISR2 X offset against the spacecraft potential (see Figure 20). We can see a clear cluster of points around 1.3 mV/m corresponding to the primary peak of the distribution. The main cause of broadening is due to data with ASPOC on, which can be easily identified as a cluster of points at the spacecraft potential of -7 V.

In the production of the magnetospheric data we use two sets of offsets: in the dense plasma (SC potentials above -8 V) we use the "solar wind/magnetosheath" offsets and in low density plasmas we use the "magnetospheric" offsets. The values of the offsets applied together with

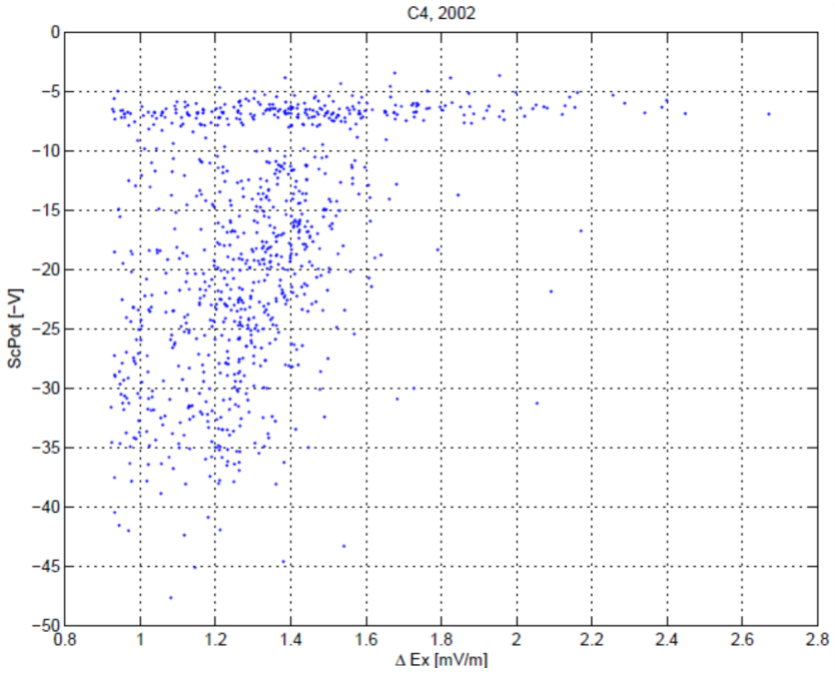

Figure 20: Sunward offset vs spacecraft potential (Cluster 4, June-November 2002).

corresponding time intervals are given in the FILE_CAVEATS section in the CEF files for the electric field data. The offsets are typically updated every several months following the spacecraft maneuvres, etc.

6.2 Comparison of E measured by EFW vs other instruments

Here, we present a summary of a study comparing electric field data in the CSA measured by the EFW with EDI, CIS-HIA, CIS-CODIF, and PEACE to evaluate the data quality resulting from the current production procedure used by the EFW team. We used 20 events covering different regions along the Cluster orbit and present the electric field and convection velocity components measured by different instruments in a standard format. We conclude that EFW, as expected, provides the highest quality electric field measurements in the spacecraft spin plane.

6.2.1 Methodology and dataset

We compare the CSA Cluster EFW measurements with those of EDI (CX_CP_EDI_MP), CIS-HIA (CX_PP_CIS,), CIS-CODIF (CX_CP_CIS-CODIF_HS_H1_MOMENTS, CX_CP_CIS-CODIF_LS_H1_MOMENTS) and PEACE (CX_CP_PEA_MOMENTS). For each event, there is at

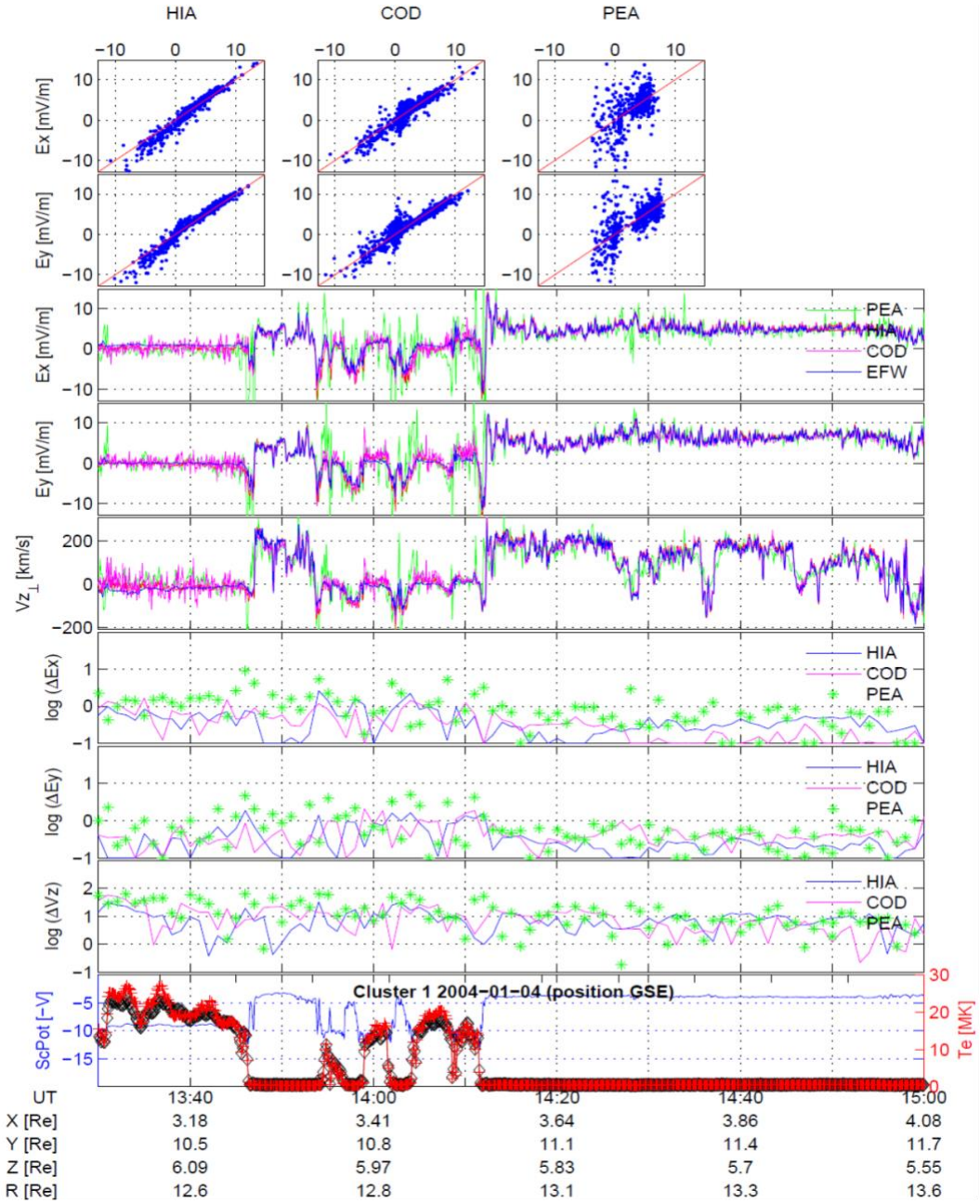

Figure 21: Cluster 1 at the magnetopause. EFW vs HIA, CODIF and PEACE.

least one “standard” plot of the above-described data for each available instrument. For most events, there are plots for both C1 and C3. C2 was not included since CIS is not operational, and C4 was not included since EDI and CIS-HIA are not operational. It should be mentioned that EFW data is routinely cross-calibrated between the spacecraft, and it is sufficient to show only C1 and C3.

For many events, there are also “fine” plots, where one or more relevant instruments have been selected to highlight good or bad agreement. On these plots, the top three line plot panels may have a somewhat different format. Data from instruments other than EFW may be plotted as Max and Min instead of a line plot. This Max-Min envelope of the particle instruments may be plotted in two ways: either as two lines indicating the maximum and minimum envelope of the data, or as a shaded area showing the same. The color coding is given in the top panel. The envelope of the data has been calculated at 1-minute time resolution for EDI, HIA, and COD, and at 4-minute time resolution for PEA.

6.2.2 Plot format

The plots contain up to 8 panels: at the top, scatter plots of data vs data; followed by 7 plots of data vs time. An example plot for a magnetopause crossing is shown in Figure 21.

The scatter plots at the top show EFW on the x-axis vs. another instrument (EDI, HIA, COD, or PEA) on the y-axis. The EFW data have been resampled to the time resolution of the other instrument. The top panel is Ex, and the bottom panel is Ey. A red line through the origin with slope 1 has been included for reference.

The next three panels show line plots of Ex, Ey, and Vzperp (= ExB/B2) for all available instruments. The color coding is given in the top panel. EFW, HIA, COD, and PEA are plotted as lines, while EDI is plotted as points. Each instrument is plotted with its own time resolution.

The next three panels show plots of the time-averaged (1-minute) difference between EFW and the other instruments on a logarithmic scale. For example, the blue line shows the difference between EFW and HIA, computed as log(abs(time_average(Ex[EFW]-Ex[HIA]))). Ex and Ey are measured in mV/m, and Vz is measured in km/s. The scale is 0.1-100 mV/m for E and 0.1-1000 km/s for V. The EFW data are resampled to the particle data time resolution before computing the differences. EFW-HIA and EFW-COD are plotted as lines, while EFW-PEA and EFW-EDI are plotted as points.

The bottom panel contains, for reference, the spacecraft potential measured by EFW (blue) together with the electron temperature measured by PEACE (red = perpendicular, black = parallel). The spacecraft number and date are given in the bottom panel. The spacecraft coordinates below the plot are in GSE.

6.2.3 Conclusions

We have presented a comparison of the CSA EFW electric field to EDI, CIS-HIA, CIS-CODIF, and PEACE. We conclude that EFW generally provides the best-quality measurement of the electric field. Normally, the statistical difference between the electric fields measured by EFW and other instruments lies within 1 mV/m, provided the measurements by other instruments are reasonable at all.

The observed differences between EFW and the other instruments are usually due to higher noise and offsets in the EDI and particle instruments. However, in some cases, the difference may be caused by spurious fields measured by EFW, which cannot be corrected by applying offset corrections to the data.

We find that generally EFW best agrees with CIS-HIA. CIS-CODIF has a much larger noise level and offset in the Z direction than CIS-HIA (especially CIS-CODIF on C3). On the other hand, we find that in some cases CIS-HIA does not follow the large electric field variations that are seen by EFW, PEACE, and CODIF. We also found cases when HIA and CODIF data differ by a constant factor.

We find that PEACE moments have very limited use inside the magnetosphere. However, there is a good agreement between EFW and PEACE in the magnetosheath, especially when the SC is in the burst mode.

EFW-EDI comparisons, in some cases, show remarkable agreement down to 0.1 mV/m in quiet fields. However, in more active regions, EDI has much more scatter, which is expected. In general, the agreement between EFW and EDI is very good.

Finally, we conclude that we see the expected picture: the quality of the electric field measured by the different instruments strongly depends on the plasma environment. We usually find a statistical agreement between EFW and at least one of the other instruments within 1 mV/m. Provided that the measured field is real, EFW generally provides the best measurement of the electric field. The production procedure used by the EFW team results in

high data quality.

More information about this study can be found in "Cross-Calibration study", see references.

7 Summary

Processing of EFW data for the CSA is a complex procedure that requires a number of calibration and cross-calibration steps, during which different offsets are determined.

7.1 Raw data and calibration parameters

The calibration parameters determined during the data processing, as well as some instrument settings values and raw data signals, are available as ancillary datasets (for details, see the EFW ICD).

Sampling rate	CSA Dataset name	Description
5 s^{-1}	C[n]_CP_EFW_L1_P1	Potential, Probe 1 to spacecraft (raw data)
	C[n]_CP_EFW_L1_P2	Potential, Probe 2 to spacecraft (raw data)
	C[n]_CP_EFW_L1_P3	Potential, Probe 3 to spacecraft (raw data)
	C[n]_CP_EFW_L1_P4	Potential, Probe 4 to spacecraft (raw data)
25 s^{-1} or 450 s^{-1}	C[n]_CP_EFW_L1_P12	Potential, Probe 1 to Probe 2 (raw data)
	C[n]_CP_EFW_L1_P32	Potential, Probe 3 to Probe 2 (raw data)
	C[n]_CP_EFW_L1_P34	Potential, Probe 3 to Probe 4 (raw data)
0.25 s^{-1}	C[n]_CP_EFW_L3_DER	Electric Field offsets (4 second resolution)
0.25 s^{-1}	C[n]_CP_EFW_L3_SFIT	Spinfits of the electric field from the individual probe pairs
1/32 s-1	C[n]_CP_EFW_L2_HK	Instrument settings

The Level 1 datasets (first 7 rows above) are the ***raw data*** from the instrument, decommutated and converted to physical units. **P1**, **P2**, **P3**, and **P4** are the potentials of the four individual probes, measured relative to the spacecraft. **P12**, **P34,** and **P32** are potential differences between pairs of probes. Notice that the spacecraft attitude and orbit parameters, as well as the sun reference pulse, all needed for the interpretation of the raw signal, are given in the CSA spacecraft auxiliary datasets (see Laakso, 2011).

C[n]_CP_EFW_L3_DER is the DC offset in the raw data. See section 6.1 for more information. DER is a vector with 2 components and, depending on which probes are available for E-field measurements, contains either the offsets in p12 and p34 or the offsets in p32 and p34.

7.2 Long-term evolution of offsets

Figure 22 shows the evolution of Delta offsets (difference between ISR2 E measured by probe pairs 12/32 and 34). Variations in the offset are caused by several factors. First is the solar cycle. One can see that the offset is rather small and steady at the beginning of the mission and starts to grow with the approach of the solar minimum, reaching its maximum in spring 2006. This behavior is caused by non-optimal bias current settings, and the situation was

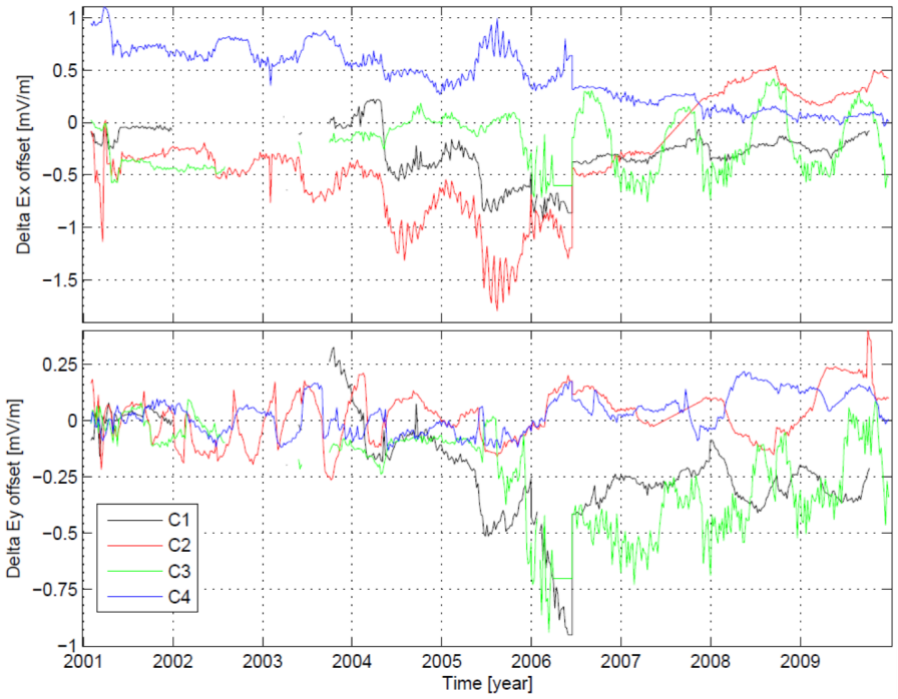

Figure 22: Evolution of delta offsets

significantly improved by lowering the bias current in June 2006. The second cause is the probe failures, which forced the usage of P32 instead of P12. P32 is of lower quality because it is not symmetric with respect to the spacecraft.

The evolution of ISR2 (DSI) offsets in the solar wind and magnetosheath during the mission lifetime is shown in Figure 23. One can see that the offsets are rather steady and slowly decreasing with the approach of the solar minimum (~2009). The only striking feature is the sudden increase in the offset on C3 in 2005. This change is not yet understood.

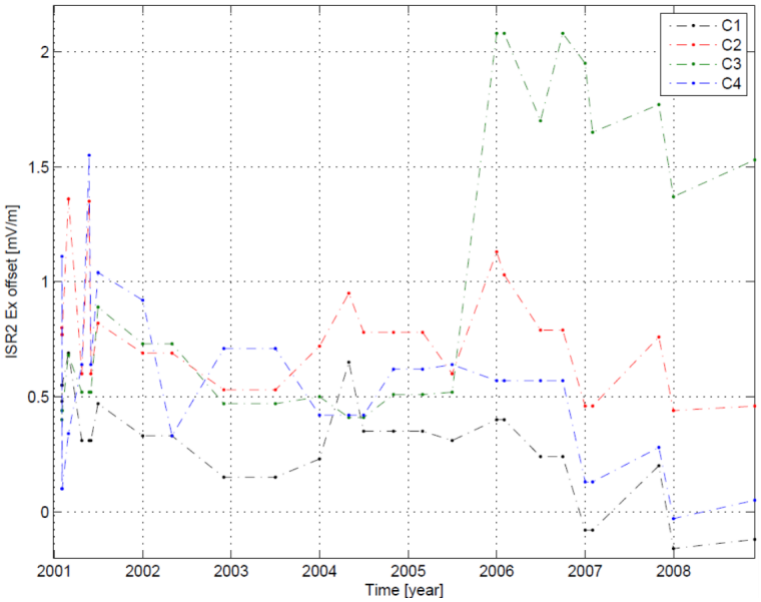

Figure 23: Evolution of ISR2 (DSI) offsets in the SW/MSH

Evolution of ISR2 offsets in the magnetosphere during mission lifetime is shown in Figure 24. The offsets are steady and slowly decreasing with the approach of the solar minimum.

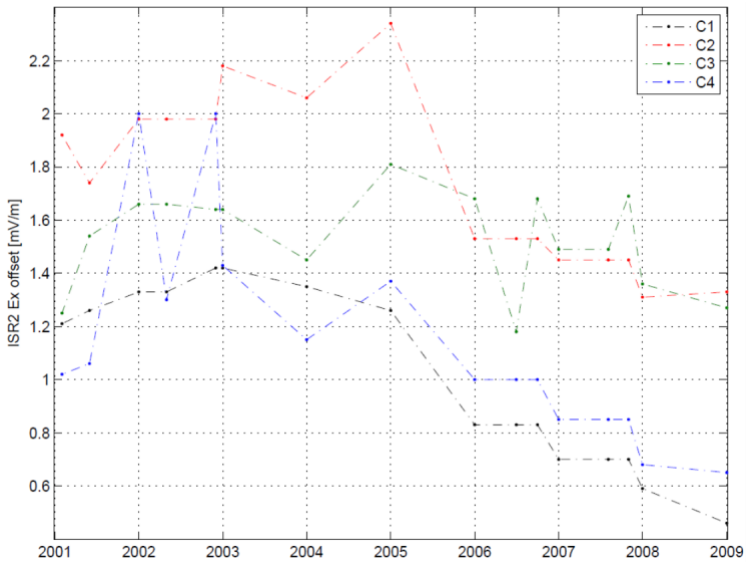

Figure 24: Evolution of ISR2 (DSI) offsets in the magnetosphere

8 References

EFW “non-standard operations” database (caveat dataset C[1-4]_CQ_EFW_INST).

Cully C. M., R. E. Ergun, and A. I. Eriksson, Electrostatic structure around spacecraft in tenuous plasmas, J. Geophys. Res. 112, A09211, doi:10.1029/2007JA012269, 2007.

Gustafsson, G., R. Boström, B. Holback, G. Holmgren, A. Lundgren, K. Stasiewicz, L. Åhlén, F. S. Mozer, D. Pankow, P. Harvey, P. Berg, R. Ulrich, A. Pedersen, R. Schmidt, A. Butler, A. W. C. Fransen, D. Klinge, M. Thomsen, C.-G. Fälthammar, P.-A. Lindqvist, S. Christenson, J. Holtet, B. Lybekk, T. A. Sten, P. Tanskanen, K. Lappalainen, and J. Wygant, The Electric Field and Wave Experiment for the Cluster Mission, Space Sci. Rev. 79, 137-156, doi:10.1023/A:1004975108657, 1997.

Engwall, E., A. I. Eriksson, and J. Forest, Wake formation behind positively charged spacecraft in flowing tenuous plasmas, Phys. Plasmas 13, 062904, doi:10.1063/1.2199207, 2006.

Eriksson, A. I., M. André, B. Klecker, H. Laakso, P.-A. Lindqvist, F. Mozer, G. Paschmann, A. Pedersen, J. Quinn, R. Torbert, K. Torkar, and H. Vaith, Electric field measurements on Cluster: comparing the double-probe and electron drift techniques, Ann. Geophys. 24, 275-289, 2006.

Eriksson, A. I., Y. Khotyaintsev, and P.-A. Lindqvist, Spacecraft wakes in the solar wind, In Proceedings of the 10th Spacecraft Charging Technology Conference (SCTC-10), doi:10.48550/arXiv.2603.12860, 2007.

Laakso, H. Cluster Active Archive – User Guide, CAA-EST-UG-0001, 2011.

Lindqvist, P.-A. and Y. Khotyaintsev, Cluster Active Archive: Interface control document for EFW, ESA document CAA-EFW-ICD-0001, doi:10.5270/esa-rp1zebe, 2026.

Lindqvist, P.-A., C. M. Cully and Y. Khotyaintsev, User Guide to the EFW measurements in the Cluster Active Archive (CAA), ESA document CAA-EST-UG-EFW, doi:10.5270/esa-rp1zebe 2026.

Puhl-Quinn, P. A., H. Matsui, V. K. Jordanova, Y. Khotyaintsev, and P.-A. Lindqvist, An effort to derive a convection electric field model in the inner-magnetosphere: Merging Cluster EDI and EFW data, J. Atmosph. Solar-Terr. Phys., 70, 564-573, doi:10.1016/j.jastp.2007.08.069, 2008.

Shue, J.-H., J. K. Chao, H. C. Fu, C. T. Russell, P. Song, K. K. Khurana, and H. J. Singer, A new functional form to study the solar wind control of the magnetopause size and shape, J. Geophys. Res., 102, 9497-9512, doi:10.1029/97JA00196, 1997.